ELSEVIER

Journal of Electron Spectroscopy and Related Phenomena 84 (1997) 159–169

JOURNAL OF ELECTRON SPECTROSCOPY and Related Phenomena

High-resolution X-ray absorption microspectroscopy of lamellar phases in natural ilmenite

T. Droubay[a], G. Mursky[b], B.P. Tonner[a,*]

[a]*Department of Physics, University of Wisconsin–Milwaukee, PO Box 413, Milwaukee, WI 53201, USA*
[b]*Department of Geosciences, University of Wisconsin–Milwaukee, PO Box 413, Milwaukee, WI 53201, USA*

Received 29 May 1996; accepted 5 January 1997

Abstract

X-ray absorption microscopy is used to study the surface of a mineral, ilmenite. High-quality surface-sensitive micrographs are easily obtained without special sample preparation beyond that usually used in preparing samples for optical microscopy. The X-ray micrographs show an expected lamellar domain structure that has a very strong contrast change at the iron and titanium L-edges. High-resolution spectroscopy from these two different regions reveals fine structure from iron atoms in two different charge states, and titanium in a single phase. A theoretical analysis and curve-fitting procedure is used to determine the precise stoichiometry of the structures in the two phases detected. These results show that quantitative surface chemistry studies can be performed on natural mineral samples using X-ray photoelectron emission microscopy. © 1997 Elsevier Science B.V.

Keywords: X-ray absorption microspectroscopy; X-ray photoelectron emission microscopy; Ilmenite; Surface chemical analysis

1. Introduction

This article reports our findings in an application of a new technique for surface chemical analysis, X-ray absorption microscopy, to the study of the natural mineral ilmenite. This mineral forms lensoid exsolution bodies of hematite phases in a lamellar structure which is well known, and thereby serves as an appropriate system for testing the application of a new method of surface analysis.

Ilmenite, which has a nominal composition of $FeTiO_3$, is a constituent of black sands found in association with magnetite (Fe_3O_4), rutile (TiO_2), zircon and monazite. It is a major source of titanium, and is used principally in the manufacture of titanium dioxide for paint pigments, replacing lead compounds. The mineral is interesting for a number of geophysical reasons, and has interesting magnetic properties as well. Ilmenite forms solid solutions with hematite (Fe_2O_3). Phases in the ilmenite–hematite solid solution series are important sources of terrestrial magnetism, and the magnetic properties of some compounds in the series are important in paleomagnetic research, because of the presence of stable remanence [1].

Ilmenite in natural rocks is known to form lamellar structures in proximity with other spinel phases, including magnetite and hematite [1–3]. This makes for a richly complex surface with a range of chemical compositions. The magnetic properties of the component compounds are also complex and varied. In

* Corresponding author. Tel.: +1 414 229 4626; fax: +1 414 229 5589; e-mail: tonner@csd.uwm.edu

PII S0368-2048(97)00018-2

ilmenite, both the Fe and Ti atoms occupy octahedral cation positions, as in the corundum structure. Along the c-axis, the Fe^{2+} and Ti^{4+} atoms are ordered in alternating planes. The iron atoms are ordered antiferromagnetically across the intervening Ti planes, and the magnetic unit cell is twice the lattice spacing along the c-axis. Hematite, often found in conjunction with ilmenite, is antiferrimagnetic. Fe^{3+} atoms within a given plane are ferromagnetically aligned, but coupled antiferromagnetically to neighboring planes. The coupling is imperfect, leading to a small net ferromagnetic moment at room temperature. The direction of ordering in hematite is temperature dependent. Above 263 K (Morin transition) the alignment is perpendicular to the c-axis, below this temperature the alignment rotates to parallel to the c-axis. Brown et al. [1] have studied the magnetic phase diagram of artificial hematite–ilmenite solid solutions.

There are a number of motivations for our application of X-ray absorption microscopy to geological problems. X-ray absorption fine-structure spectroscopy (XAFS) has characteristics that make it very attractive for studying minerals, which have complicated chemical compositions. In particular, the XAFS spectrum gives highly detailed information about the charge state and coordination of both cations and anions. The near-edge absorption spectrum is very sensitive to small distortions in the local symmetry of the absorbing atom. This kind of detail is needed in the study of geological materials, where many different mineral structures may have the same nominal stoichiometry [4]. There is, additionally, the nearly unique opportunity to study charge-state specific magnetic properties, as reflected in the X-ray magnetic dichroism with both circularly and linearly polarized light. With circular polarization, ferromagnetic domains are detected. With linearly polarized light, local magnetic moments [5], and antiferromagnetic ordering [6], can be determined. Both effects are compatible with spatial resolution in X-ray absorption microscopy [7]. This new technique can be used to study the distribution of magnetic phases at high spatial resolution in geological samples.

With the high spatial resolution now attainable in XAFS microscopy, a number of new avenues of research with complex samples like geochemical surfaces can be envisioned. There are potentially many examples in which the mapping of the distribution of phases in natural materials will be aided by this technique, which has unique characteristics and does not require ultrathin samples. The method can be applied to natural samples prepared in a number of ways, including polished or cleaved surfaces, or to exposed surfaces of small particles from soils ranging from hundreds of microns down to submicron dimensions. In addition, the surface sensitivity inherent in XAFS microscopy with secondary yield detection makes it attractive to consider the study of surface reactions on complex materials, where the differences in reaction rates and products could be studied on individual grains of varying composition in a natural material.

We consider here the XAFS spectra of Fe and Ti L-edges, for which a reasonable body of theoretical and experimental work is available on model compounds. It is possible to use XAFS at the transition metal L-edges to determine site occupancy, valence charge, and coordination of the absorbing atom. A prerequisite for this is to have both excellent energy resolution and well-understood detection methods, since the detailed line shape must be accurately measured to analyze these effects. In order to have good spatial resolution and spectral resolution simultaneously, along with a reasonable image intensity, it is beneficial to have a high-brightness X-ray source and a high-resolution grating monochromator. These conditions have been met by using a new undulator X-ray beamline at the Advanced Light Source [8].

2. X-ray photoelectron emission microscopy

X-ray absorption spectroscopy can give information both about the local geometric structure and the density of unoccupied orbitals near a particular atomic site, which is identified by the energy of the absorption edge. The near-edge spectrum [9] is a site-specific probe of local charge state, coordination, and magnetic moment, and is roughly the region of up to 50 eV from the absorption edge. Above this energy, oscillations in the absorption cross-section are called the extended fine structure, and are caused by reflections of the photoelectron wave from neighboring atoms. These types of absorption fine structure are related, and can be generically referred to as X-ray

absorption fine structure (XAFS). We are only concerned with near-edge results in this report. However, all of the methods used are equally suited to measuring the extended fine structure.

A number of different detection methods are possible for XAFS experiments, ranging from transmission through thin films to detection of fluorescent yield. We use the method of secondary electron yield detection, which is directly compatible with microscopic imaging in the X-ray photoemission electron microscope (XPEEM) [10,11]. Briefly, this technique uses an electrostatic electron microscope to image the photoemitted secondary electrons. Magnified images are projected onto an image intensifier, and captured by a digital video camera system. XAFS spectra are taken by scanning the incident photon energy, and recording the intensity from selected areas of the sample surface as a function of photon energy. In most cases, it is valid to assume that the measured secondary electron yield is directly proportional to the absorption coefficient, although a more exact treatment may be necessary in special cases [12]. Secondary yield detection is not as surface sensitive as photoemission spectroscopy, ranging from about 15 Å in transition metals [13] to up to 100 Å in carbon layers [13]. This can be an advantage, since it enables you to "see" through a contamination layer without resorting to ion sputtering, which might alter the surface composition. Sensitivity is still high enough to measure strong signals from submonolayer coverages of adsorbates [14].

Our sample consisted of a polished surface of a natural ilmenite mineral specimen. The surface preparation was standard mechanical polishing, followed by rinsing in water and organic solvents. No further surface preparation was needed to produce high-intensity X-ray micrographs. In optical micrographs, the surface consisted of regions that were flat over a few hundred microns, separated by various large pores and scratches. These large surface defects did not affect the quality of the X-ray micrograph. In Fig. 1 we show a series of XPEEM micrographs of the surface of the ilmenite sample. The first two images are taken at the Fe L-edge (near 708 eV) and the Ti L-edge (near 465 eV), respectively. The third image is a difference image made from the first two.

The micrographs at the two edges show interesting effects, which are traced to the energy dependence of contrast in XPEEM images. In photoemission electron microscopy, the image contrast at any given incident photon energy arises from a number of factors, including surface topography, variations in crystallite orientation, work function changes, and differences in chemical composition [11]. The surface morphology effects are constant as the photon energy is changed, and since the incident energy is well above the work function in XPEEM, the main contrast variation with photon energy is due to compositional variations. At the Fe edge (Fig. 1(a)), the specimen surface is seen to have two distinct regions, a background region which appears grey, and a set of vertical striped domains of various thickness which appear at higher intensity. At the Ti L-edge (Fig. 1(b)) the contrast between the striped regions and the background reverses. This effect is highlighted in Fig. 1(c), which shows the difference image. The difference image suppresses the topographical features and brings out the photon energy-dependent contrast of the chemically distinct regions in the stripes and background areas.

The origin of this contrast is clearly elemental, having to do with the distribution of Fe and Ti in the sample. By comparing the relative yield between the striped domains and the background at both the Fe and Ti edges, we can conclude that the stripes contain excess Fe compared to background, and a deficiency of Ti. It is known that layered structures occur in the phase separation of ilmenite from hematite and magnetite [2], and we see a similar lamellar structure in the X-ray micrograph. A range of lengths of the lamellae is visible in the micrograph, ranging from the two large stripes of 5–10 μm width, down to 1 μm or less in width in the background region. The sample surface contained many areas that had a similar distribution of lamellae, and other regions with more rectangular domains.

Although qualitative judgments like this (excesses and deficiencies of one or more elements) can be deduced from a set of energy-dependent micrographs, it is not possible to quantify the elemental distribution from such data. This is not a practical limitation, but rather a fundamental one, since the absorption edge intensity rides on top of a background, which varies from point to point in the image. At the least, two images just below and above the edge should be compared, to extract quantitative distributions of elements. At another, very desirable, extreme the

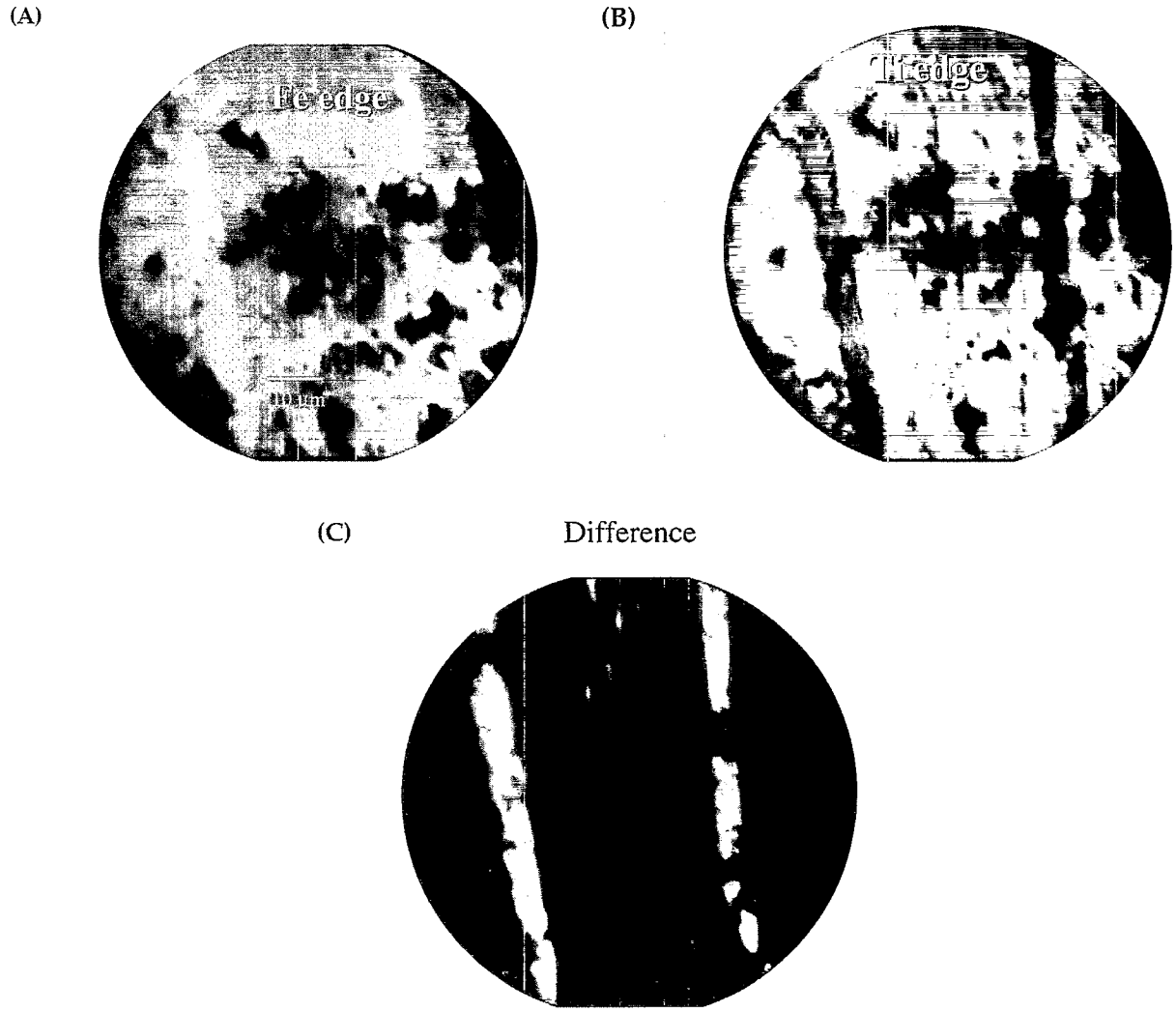

Fig. 1. XPEEM micrographs of the ilmenite surface at photon energies of (a) 708 eV, near the maximum of the Fe L_3-edge, and (b) 465 eV, near the maximum of the Ti L-edge structures. (c) Difference image of the first two to highlight the lamellar structure of chemical domains. For reference, the two types of domain are called "on-stripe" and "off-stripe."

entire image could be acquired as a function of incident photon energy, for small steps in energy. This would produce an XAFS spectrum for every pixel in the image. This is the ultimate goal, and basic meaning, of spectromicroscopy [11]. Since the XAFS spectrum contains much more information than just elemental distribution, a complete spectromicroscopy data set would produce high-resolution maps of charge-state distribution and coordination.

In practice, hardware and software limitations restricted us to a less complete, but still very useful, strategy. By observing a set of images taken at photon energies between the Ti and Fe L-edges, we were able to determine that the sample contained two dominant chemical compositions, represented by the bright stripes and grey background areas in Fig. 1. Throughout the remainder of this report, we will refer to these two types of domain as "on-stripe" and "off-stripe." Rather than accumulate spectra at every single pixel in the image, we instead acquire the XAFS spectrum from a selected set of areas on the sample surface (microspectroscopy). Data from three areas within

the stripes, of 5 μm diameter, and three areas off the stripes, were averaged together to produce a "representative" spectrum. There were small, but noticeable, differences in the XAFS data from small region to small region, indicating that the stripes were not entirely chemically homogeneous. These variations were small, however, compared to the difference between "on-stripe" and "off-stripe".

The XAFS spectra at the Fe edge from ilmenite are shown in Fig. 2, along with a micro-XAFS spectrum from a geological sample of magnetite for comparison. The spectra have been background subtracted and normalized to have the same (unity) edge–jump intensity at 730 eV, a per-atom normalization [9]. The Fe L-edge spectrum is characterized by two peak manifolds, at the L_3 ($2p_{3/2}$) edge near 705 eV, and the L_2 ($2p_{1/2}$) edge near 716 eV. In pure Fe metal, the edges appear as two broad peaks at the L_3 and L_2 positions [15]. In compounds, the presence of the crystal field and spin–orbit effects causes a large splitting of the lines at the two edges, and multiple peaks can be seen. Two large peaks, and one smaller shoulder (Fig. 2(b), near 705 eV), are obvious to the eye at both the L_2 and L_3 edge in oxides. The two large peaks arise from contributions from Fe in the Fe^{2+} and Fe^{3+} charge states, indicated by the vertical dashed lines in Fig. 2. It requires relatively high spectral resolution (0.3 eV or better) to adequately separate these features.

The XAFS spectra at the Ti L-edge, for the "on-stripe" and "off-stripe" domains, are shown in Fig. 3. The spectra from the two compositional domains are essentially identical. A comparison to spectra from reference compounds of titanium oxides shows substantial differences (see below), so we identify the Ti spectrum as originating entirely from the ilmenite component of the sample.

In contrast, there are large differences present in the Fe edge spectra of the "on-stripe" and "off-stripe" region. It is clear that these are related to a difference in the Fe^{2+}/Fe^{3+} charge-state ratio, which is in turn due to the presence of multiple phases in the sample. The next section deals with a theoretical analysis of the spectra and a quantitative determination of this charge-state ratio. The spectrum from magnetite, Fe_3O_4, is also shown. It has two strong peaks at both the L_3 and L_2 edges, which are due to the Fe^{3+} and Fe^{2+} sites in magnetite [16]. There are significant

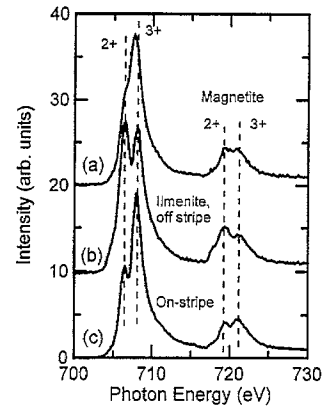

Fig. 2. X-ray absorption spectrum of the Fe L-edge from the two types of domains seen in the micrograph of Fig. 1, called "on-stripe" (c) and "off-stripe" (b). The spectra have been normalized to the same edge–jump ratio (per-atom basis), to highlight the fine structure differences between the two regions. Also shown in (a) is the spectrum from magnetite for comparison. The main L_3-edge peak in magnetite is at a slightly different energy from that of the ilmenite sample. The broken lines indicate the strongest features due to Fe in the 2 + and 3 + charge states.

differences between the magnetite and ilmenite spectra however, such as a shift in energy of the 3 + peak at the L_3 edge, and a completely different relative intensity of the component lines at both edges. These differences at the Fe edge, and the single-phase spectra at the Ti edge, lead us to restrict our model of the composition of the specimen surface domains to include only ilmenite ($FeTiO_3$) and hematite (Fe_2O_3) phases.

3. Composition analysis by quantitative XANES

Theoretical work on calculating X-ray absorption near-edge structures is extensive. For the L-edges of transition elements, a range of treatments can be found in the literature, including atomic models [16–20], an LCAO band-structure model [21], and a local density functional approach [22]. The transition metal L-edges of oxides have been studied theoretically using atomic calculations to determine the multiplet splittings in intermediate coupling limits, with a resulting fair to good agreement with experiment [16–20]. These calculations also correctly reproduce the variation in branching ratio across the first-row transition element series [17], which is a large effect that is

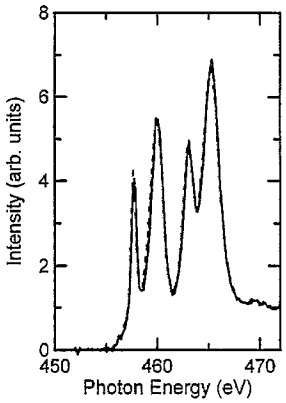

Fig. 3. X-ray absorption spectrum from the two domains shown in the micrograph of Fig. 1, for the Ti L-edge region. No significant fine-structure intensity difference is found, indicating a uniform chemical state for Ti throughout the sample. The Ti edge intensity difference must therefore be due to Ti concentration changes from one domain to the other. —— on stripe; - - - off stripe.

not necessarily correctly reproduced in the band-structure models [21].

Here, we are interested in accurately and precisely determining the ratio of Fe atoms in the 2 + and 3 + charge states, in the two types of domains seen by XAFS microscopy in this ilmenite sample. The main structures at the L_3 and L_2 edge (see Fig. 2) are a pair of peaks at each edge, which are separated in energy by about 1.5 eV between the two charge states. From the theoretical calculations, there is some important peak overlap between the two charge states. Specifically, the Fe^{3+} spectrum has a shoulder that lies underneath the main Fe^{2+} L_3-edge peak. In order to accurately fit the experimental spectra to a charge state model, we need theoretical spectra with the correct energy positions of the main spectral lines, and equally important, we need the correct ratio of intensities between the various lines because of the existence of peak–shoulder overlaps between the two charge states.

In this work, we use the results of an atomic model from Crocombette et al. [16], which is a configuration interaction calculation including the central cation and the surrounding nearest neighbor oxygen atoms. The calculation includes crystal field splitting, charge transfer, and spin–orbit coupling of the Fe 2p orbitals. An earlier calculation by van der Laan and Kirkman [19] of Fe in both octahedral and tetrahedral symmetry, including both crystal field and spin–orbit interactions, was also considered. The two calculations had similar intensities for the main L_3 and L_2 peaks, although differences could be distinguished. These differences were smaller than the dominant discrepancies between theory and experiment, discussed below, so we do not believe the results would be significantly different between one or the other choice of theoretical models.

The initial state spin–orbit splitting is large in Fe, so that the theoretical eigenvalues are easily separated into two families of lines at the L_3 and L_2 edges. Since the experimental resolution (about 0.3 eV) and the intrinsic linewidth (0.2 and 0.4 eV at the L_3 and L_2 edges) broaden the spectrum, it is possible to model the theoretical spectrum with an empirical set of Gaussian peaks. We use a Gaussian set of 11 peaks to model the Fe^{2+}, and 10 peaks for the Fe^{3+} spectrum in octahedral symmetry (see Table 1).

The parameters shown in Table 1 were used to create model theoretical spectra for curve fitting the experimental XAFS data. We used data appropriate for Fe in octahedral sites in Fe_3O_4 clusters. These parameters are modified slightly from those which produce the best fit to the theory of [16]. These changes were the following. The absolute energy position of the theoretical spectrum was shifted to the best fit to experiment, keeping the relative positions of the peaks fixed at the original theoretical value. A shift of 0.9 eV to lower energy was applied to the Fe^{2+} theory, relative to Fe^{3+} , which is consistent with the value of 0.7 eV found in the original work [16]. The second modification made was to increase the branching ratio by about 5% over the original values, as shown in Table 1. This was done while keeping the integrated area of the theoretical spectrum constant, so that the ratio of d-holes in the Fe^{2+} and Fe^{3+} spectra was properly maintained at the theoretically predicted values of 3+:2+ = 4.57:3.69 [16]. The most likely reason for the required increase in branching ratio is the uncertainty in the shape of the background under the L_3 and L_2 edges.

For fitting to experimental data, we introduce a background intensity, $I_B(E)$, which is calculated as

$$I_B(E) = \frac{1}{N}\int_{E_{MIN}}^{E} I_M(e)de \qquad (1)$$

Table 1
Values used in the theoretical spectrum for Fe^{2+} and Fe^{3+}, octahedral symmetry[a]

Fe^{2+}(octahedral)	Peak 2	Peak 3	Peak 4	Peak 5	Peak 7	Peak 8	Peak 9
Energy	704.95	706.48	707.7	709.4	717.8	719.4	720.49
Height, H	0.328	1.09	0.498	0.2	0.137	0.269	0.151
Width, W	0.436	0.436	0.592	0.632	0.592	0.469	0.5
Int. area (d-holes)	3.69						
Branching ratio[b]	0.77 (0.73)						
Fe^{3+}(octahedral)	Peak 1	Peak 2	Peak 3	Peak 4	Peak 5	Peak 7	Peak 8
Energy	706.51	708.1	709	709.8	711.6	719.7	721.3
Height, H	0.593	1.445	0.301	0.271	0.211	0.18	0.269
Width, W	0.418	0.5	0.548	0.592	0.707	0.566	0.592
Int. area (d-holes)	4.58						
Branching ratio[b]	0.81 (0.75)						

[a] Data for the strongest 7 peaks are included, leaving out intensities below 0.1; 11 peaks total were used to fit the Fe^{2+} state, and 10 were used for the Fe^{3+} state. The Gaussian peaks are of the form $I = H\exp(-\Delta X^2/2W^2)$.
[b] Theoretical value given in parentheses.

where the normalization factor, N, is defined so that the background equals unity above the edge, $I_B(E_{MAX}) = 1$, which is the convention used for displaying the experimental data, $I_M(e)$. The integration endpoints, $E_{MIN} = 700$ eV and $E_{MAX} = 730$ eV are chosen to be well below and above the edge. This background has the advantage that it is directly computed from the experimental data, and therefore requires no assumptions to be made about the shape of the background intensity. In practice, it produces edge–jump ratios at the L_2 and L_3 edges that are smaller than either the statistical value (1:2) or the value expected from the branching ratio. We believe this leads to an overestimate of the branching ratio in our fit, as mentioned above.

Our choice of theoretical modeling spectra is motivated by wanting to maintain a self-consistent method of curve fitting, which requires that the ratio of the intensities in the Fe^{2+} and Fe^{3+} channels be quantifiably related. What this means in terms of the fitting functions is that the "white line ratio," that is, the relative intensity of the d-hole absorption spectrum to the background, must be in some proportion for the two charge states that can be independently verified. In our case, we have kept the white line ratio fixed for the two charge states, as taken from the theory.

As a first test of the validity of these theoretical fitting functions, we show, in Fig. 4, a comparison of the best fit to our experimental magnetite spectrum (Fe_3O_4), which contains 33% of the Fe in the octahedral 2 + charge states. The bottom curves of Fig. 4 show the theoretical composite spectra for the two charge states, and the solid curve at the top is shown with the experiment (dots). The relative contribution of the two theoretical spectra was varied in a standard linear fit, and the best fit determined from a standard least-squares R-factor, shown in Fig. 5. The best fit gives a value of 36% atomic per cent Fe^{2+}, close to the expected value of 33%, with a well-shaped quadratic R-factor indicating an uncertainty of about 5%. Given a number of problematic issues in the curve fitting, discussed in detail below, we believe this is the limit of accuracy attainable using the present set of theoretical parameters.

Although the quality of fit shown in Fig. 4 is reasonable, there are a number of problem areas that could be improved in future work. In the original work of Crocrombette et al. [16], they fit a magnetite spectrum using Fe^{3+} spectra for clusters with tetrahedral and octahedral symmetry sites in equal proportion, according to the correct distribution of sites in this compound. However, the quality of best fit is significantly worse than what we achieve using only the octahedral symmetry spectra. The difficulty is that the theoretical spectra grossly underestimate the first peak in the Fe^{3+} L_3 edge (near 706.5 eV), which is close to the main peak in the Fe^{2+} spectrum

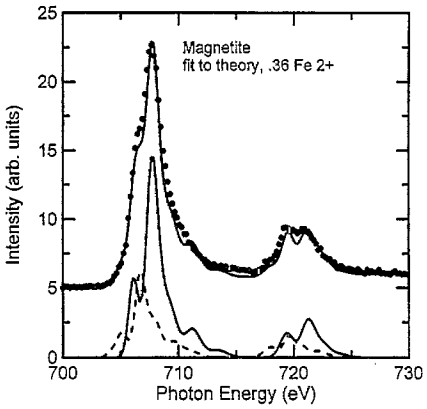

Fig. 4. Top: a high-resolution XPEEM spectrum from natural magnetite, Fe_3O_4, shown as the dots, and a simulated spectrum which is the best fit sum of the theoretical spectra for Fe^{2+} and Fe^{3+}. Bottom: theoretical component spectra for the 3 + (solid) and 2 + (dashed) charge states. The peak shapes at both the L_2 and L_3 edge are strongly dependent on the charge state.

and therefore has a large effect on the fitting. A similar problem occurs with the Fe^{3+} octahedral site in hematite (Fe_2O_3) [16,19]. It had been argued by van der Laan and Kirkland [19] that this disagreement could be improved by including the trigonal distortion in Fe_2O_3, but the problem remains even when the correct local bond length distortions are used [16]. In the interest of maintaining an internally self-consistent fit, and considering the reasonable fitting results achieved for magnetite, we refrain from making further adjustments to the theoretical spectra, although we expect that there is much room for improvement, particularly given the fine detail seen in these high-resolution spectra.

Having found that our model theoretical spectra give reasonable results for the test case of magnetite, we applied the same models to the ilmenite domain spectra. The resultant best fits of the model spectra to experiment are shown in Fig. 6 for the "on-stripe" domains, and in Fig. 7 for the "off-stripe" domains. The *R*-factor analysis of the two cases is shown in Fig. 8. The "on-stripe" region is found to have a minority component of Fe^{2+}, which is the species present in ilmenite. The 20% atomic fraction of Fe^{2+} which is found in the stripe should be viewed as an upper-bound estimate, since corrections to the Fe^{3+} model spectrum to improve agreement between theory and experiment would reduce this number. From this fit, and the similarity of the spectrum to reference compounds, we identify the majority species in the "on-stripe" region as hematite (Fe_2O_3).

In the "off-stripe" region, which represents the

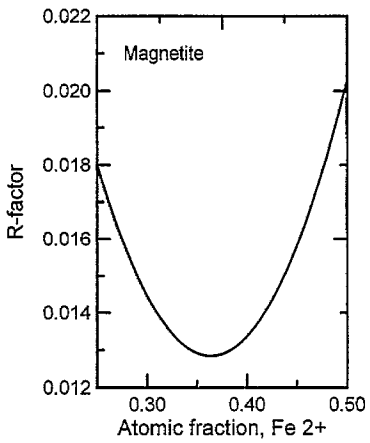

Fig. 5. *R*-factor analysis of the fit between theory and experiment for the magnetite spectrum. The experimental result is 36% Fe^{2+}, close to the stoichiometric ratio for Fe_3O_4 of 33%, serving as a validation for the use of the theoretical spectra in fitting the ilmenite data.

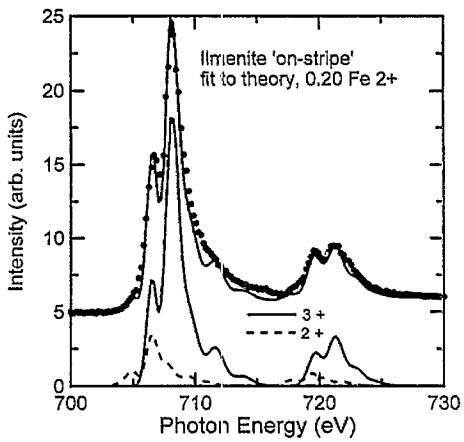

Fig. 6. Top: best fit of theoretical spectra (solid curve) to the experimental data for the ilmenite lamellar region (dots), "on-stripe". Bottom: component theoretical spectra for the 2 + (dashed) and 3 + (solid) charge states in octahedral symmetry. The best fit corresponds to 80% Fe^{3+}, assigned to the hematite phase Fe_2O_3.

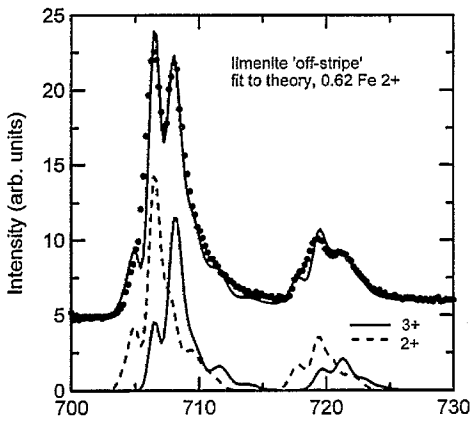

Fig. 7. Top: best fit of theoretical spectra (solid curve) to the experimental data (dots) for the "off-stripe" region of ilmenite in Fig. 1. Bottom: component theoretical spectra for 2 + (dashed) and 3 + Fe states (solid). The amount of Fe^{2+} is determined by the simultaneous fitting of the large L_2-edge peak (719 eV) which is unique to Fe^{2+}, and the magnitude of the first large peak at the L_3 edge (706 eV) which overlaps a small peak of Fe^{3+}. The best fit corresponds to 62% Fe^{2+}, in the ilmenite phase, and 38% in the Fe^{3+} hematite phase.

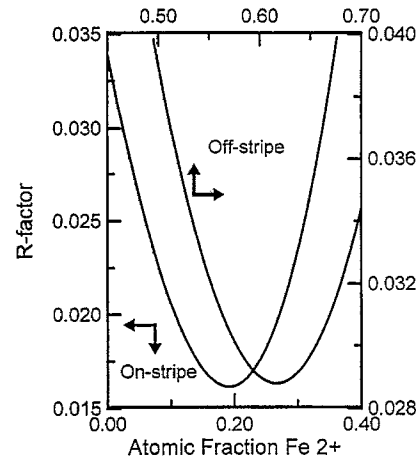

Fig. 8. *R*-factor analysis of the composition determination resulting from fitting theoretical 2 + and 3 + spectra to the measured data for the "on-stripe" and "off-stripe" regions (note two different scales used). The curves have a good parabolic shape, although the width is larger than it would be if semiempirical fitting parameters were used to better match the linewidths in the theory to the measured data.

bulk of the sample material, the dominant charge state is Fe^{2+} at 62% atomic fraction (best fit). We assign this to the iron in the ilmenite phase, with the remainder being in the hematite Fe^{3+} phase. The original micrographs show that the "off-stripe" region contains many smaller domains that appear similar to the "on-stripe" composition, but are smaller in size. The "off-stripe" spectra integrate over an area that includes these small lamellar regions of hematite, leading to a spectrum that has some finite fraction of Fe^{3+} in it.

The *R*-factor analysis (Fig. 8) has a good, parabolic, shape for both ilmenite fits, indicating a systematic uncertainty of order 5%.

The charge-state ratio for the "on-stripe" (minority) region is 3 + :2 + = 4:1, and for the "off-stripe" (majority) region it is 3 + :2 + = 2:3. If we assume the simplest, two-component, model of the two regions, the stripes are found to be mixture of $FeTiO_3$ + $2Fe_2O_3$, and the majority region corresponds to the mixture $3FeTiO_3$ + Fe_2O_3. The titanium edge spectrum (Fig. 3) is identical throughout the sample, and it does not agree with spectra for TiO_2 in anatase, brookite or rutile [20], so we exclude consideration of a third phase of precipitated titania or another Fe–Ti oxide. The striped regions have less titanium than the rest of the sample, and this, along with the quantitative charge state fitting data, supports the model that there is a simple charge state substitution of the form $2Fe^{3+} < > Fe^{2+} + Ti^{4+}$ [1,2]. With the measured charge state ratios, a charge balance equation can be written,

$$4FeTiO_3 + 8Fe_2O_3 < > 9FeTiO_3 + 3Fe_2O_3$$

where the left-hand side represents the atomic fractions in the "on-stripe" region, which has a deficit of titanium compared to the majority sample fraction, represented by the right-hand side.

4. Discussion

We have demonstrated the potential for obtaining quantitative information about charge-state distributions in natural geological materials using the X-ray PEEM and micro-XAFS. By using theoretical models of the component spectra, we are able to quantify the charge-state ratios of iron in two phases in the mineral ilmenite with a high precision. This opens the way to studies of reactions at the surfaces of complex, inhomogeneous samples found in nature.

Some improvement is possible in the choice of modeling spectra. We have noted the difficulties associated with the atomic theories not correctly reproducing the intensity of the leading peaks at both the L_3 and L_2 edges. Crocrombette et al. [16] note that this difficulty persists even when distortions from octahedral symmetry, charge transfer, and spin–orbit coupling are taken into account. Furthermore, the problem does not appear to be as large in the octahedral 2 + case, seemingly affecting only the d^5 configurations. Additional work is needed to improve the theoretical agreement to experiment in these leading-edge peaks, since they have such a large effect on the quality of the overall fit. One potential alternative is to use spectra from model compounds as the fitting curves; for example by using the hematite (Fe_2O_3) spectrum to model octahedral Fe^{3+}. To do this, a very accurate set of model spectra will be needed, to insure that the relative d-hole intensities (white-line ratios) are correctly determined.

The methods described here can obviously be implemented at other X-ray wavelengths. In some samples, we have seen strong EXAFS oscillations above the edge which can be used to determine interatomic bond lengths in individual chemical domains. Although we have concentrated on a specific example using soft X-ray light, there is no fundamental difference in technique when using higher energy X-rays, which can extend the range of materials studied and make it easier to do micro-EXAFS measurements.

The image contrast is often very strong in XPEEM. However, precautions must be taken before interpreting these intensity variations in terms of compositional differences in the sample. The complete method of spectromicroscopy will involve recording a complete image at every energy step, producing a spectrum for each pixel in the image. The microspectroscopy methods described here provide a practical intermediate data acquisition strategy when data storage space and data retrieval are concerns.

The XAFS spectrum is preferred to a photoemission spectrum in transition metal oxides, because of the enhanced sensitivity to charge state and local symmetry. It is possible to collect XAFS data using electron energy loss spectroscopy (EELS) [23], and the imaging version of this technique (TEM-EELS) is often considered as an alternative to XPEEM, which has a poorer spatial resolution. There are some significant advantages of XPEEM, however, which should be noted. These include the fact that samples do not need to be thinned, which means that very large areas of a sample can be quickly surveyed to find important or interesting regions. XPEEM is also intrinsically surface or near-surface sensitive: this will either be a crucial advantage or a disadvantage, depending on the measurement. There is also the potential for significantly less sample damage in XPEEM compared to EELS, particularly for oxides and other insulating samples [24].

Acknowledgements

These experiments were performed at the Advanced Light Source of Lawrence Berkeley National Laboratory, which is funded by the Department of Energy–Basic Energy Sciences. We would like to thank the UW-M Laboratory for Surface Studies for graduate research support. This work was supported in part by the National Science Foundation through grant DMR-9413475.

References

[1] N.E. Brown, A. Navrotsky, G.L. Nord, Jr., S.K. Banerjee, American Mineralogist 78 (1993) 941.
[2] D. Lattard, American Mineralogist 80 (1995) 968.
[3] A.F. Buddington, D. Lindsley, Journal of Petrology 5 (1964) 311.
[4] P.F. Schofield, C.M.B. Henderson, G. Cressey, G. van der Laan, Journal of Synchrotron Radiation 2 (1995) 93.
[5] W.L. O'Brien, J. Zhang, B.P. Tonner, Journal of Physics: Condensed Matter 5 (1993) L515-L520.
[6] P. Kuiper, B.G. Searle, P. Rudolf, L.H. Tjeng, C.T. Chen, Physical Review Letters 70 (1993) 1549.
[7] B.P. Tonner, D. Dunham, J. Zhang, W.L. O'Brien, M. Samant, D. Weller, B.D. Hermsmeier, J. Stohr, Nuclear Instruments & Methods in Physics Research A 347 (1994) 142-147. B.P. Tonner, Journal de Physique IV, Colloque C9, supplement au Journal de Physique III 4 (1994) C9-407.
[8] J.D. Denlinger, E. Rotenberg, T. Warwick, G. Visser, J. Nordgren, J.-H. Guo, P. Skytt, S.D. Kevan, K.S. McCutcheion, D. Shuh, J. Bucher, N. Edelstein, J.G. Tobin, B.P. Tonner, Review of Scientific Instruments 66 (1995) 1342.
[9] J. Stohr, NEXAFS Spectroscopy, Springer Verlag, New York, 1992.
[10] G. Harp, B.P. Tonner, Review of Scientific Instruments 59 (1988) 853. B.P. Tonner, G.R. Harp, S.F. Koranda, J. Zhang, Review of Scientific Instruments 63 (1992) 564.

[11] B.P. Tonner, D. Dunham, T. Droubay, J. Kikuma, J. Denlinger, E. Rotenberg, A. Warwick, Journal of Electron Spectroscopy and Related Phenomena 75 (1995) 309–332.
[12] W.L. O"Brien, B.P. Tonner, Physical Review B 50 (1994) 12672–12681.
[13] J. Stohr, M. Samant, Y. Wu, B. Hermsmeier, G. Harp, S. Koranda, D. Dunham, B.P. Tonner, Science 259 (1993) 658.
[14] W.L. O'Brien, B.P. Tonner, Physical Review B 51 (1995) 617.
[15] B.P. Tonner, W.L. O'Brien, G.R. Harp, S.S.P. Parkin, Journal of Applied Physics 76 (1994) 6462–6464.
[16] J.P. Crocrombette, M. Pollak, F. Jollet, N. Thromat, M. Gautier-Soyer, Physical Review B 52 (1995) 3143.
[17] B.T. Thole, G. van der Laan, Physical Review B 38 (1988) 3158.
[18] F.M.F. de Groot, J.C. Fuggle, B.T. Thole, G.A. Sawatzky, Physical Review B 42 (1990) 5459.
[19] G. van der Laan, I.W. Kirkman, Journal of Physics: Condensed Matter 4 (1992) 4189.
[20] J.P. Crocombette, F. Jollet, Journal of Physics: Condensed Matter 6 (1994) 10811.
[21] N.V. Smith, C.T. Chen, F. Sette, L. Mattheiss, Physical Review B 46 (1992) 1023.
[22] R. Wu, D. Wang, A.J. Freeman, Journal of Magnetism and Magnetic Materials 132 (1994) 103.
[23] R.F. Egerton, Electron Energy Loss in the Electron Microscope, Plenum Press, New York, 1986.
[24] L.A.J. Garvie, A.J. Craven, Ultramicroscopy 54 (1994) 83.